Atmos. Chem. Phys., 22, 7827–7841, 2022
https://doi.org/10.5194/acp-22-7827-2022

Atmospheric Chemistry and Physics
Open Access
EGU

Measurement report: Effects of anthropogenic emissions and environmental factors on the formation of biogenic secondary organic aerosol (BSOA) in a coastal city of southeastern China

Youwei Hong[1,2,3,4], Xinbei Xu[1,2,3], Dan Liao[5], Taotao Liu[1,2,3], Xiaoting Ji[1,2,3], Ke Xu[1,2,4], Chunyang Liao[6], Ting Wang[7], Chunshui Lin[7], and Jinsheng Chen[1,2,3]

[1]Center for Excellence in Regional Atmospheric Environment, Institute of Urban Environment, Chinese Academy of Sciences, Xiamen, 361021, China
[2]Key Lab of Urban Environment and Health, Institute of Urban Environment, Chinese Academy of Sciences, Xiamen, 361021, China
[3]University of Chinese Academy of Sciences, Beijing, 100049, China
[4]School of Life Sciences, Hebei University, Baoding, 071000, China
[5]College of Environment and Public Health, Xiamen Huaxia University, Xiamen 361024, China
[6]State Key Laboratory of Environmental Chemistry and Ecotoxicology, Research Center for Eco-Environmental Sciences, Chinese Academy of Sciences, Beijing 100085, China
[7]Institute of Earth Environment, Chinese Academy of Sciences, Xi'an, 710061, China
Correspondence: Jinsheng Chen (jschen@iue.ac.cn) and Youwei Hong (ywhong@iue.ac.cn)

Received: 21 March 2022 – Discussion started: 24 March 2022
Revised: 12 May 2022 – Accepted: 25 May 2022 – Published: 16 June 2022

Abstract. To better understand the formation of biogenic secondary organic aerosol (BSOA), aerosol samples with a 4 h time resolution were collected during summer and winter in the southeast of China, along with online measurements of trace gases, aerosol chemical compositions, and meteorological parameters. The samples were analyzed by gas chromatography–mass spectrometry for $PM_{2.5}$-bound secondary organic aerosol (SOA) tracers, including isoprene (SOA_I), α/β-pinene (SOA_M), β-caryophyllene (SOA_C), and toluene (ASOA). The average concentrations of total SOA tracers in winter and summer were 38.8 and 111.9 ng m^{-3}, respectively, with the predominance of SOA_M (70.1 % and 45.8 %), followed by SOA_I (14.0 % and 45.6 %), ASOA (11.0 % and 6.2 %) and SOA_C (4.9 % and 2.3 %). Compared to those in winter, the majority of BSOA tracers in summer showed significant positive correlations with O_x (O_3+NO_2) ($r = 0.443$–0.808), HONO ($r = 0.299$–0.601), ultraviolet (UV) ($r = 0.382$–0.588) and temperature (T) ($r = 0.529$–0.852), indicating the influence of photochemical oxidation under relatively clean conditions. However, in winter, BSOA tracers were significantly correlated with $PM_{2.5}$ ($r = 0.407$–0.867), NO_3^- ($r = 0.416$–0.884), SO_4^{2-} ($r = 0.419$–0.813), and NH_3 ($r = 0.440$–0.757), attributed to the contributions of anthropogenic emissions. Major BSOA tracers in both seasons were linearly correlated with aerosol acidity (pH) ($r = 0.421$–0.752), liquid water content (LWC) ($r = 0.403$–0.876) and SO_4^{2-} ($r = 0.419$–0.813). The results indicated that acid-catalyzed reactive uptake onto sulfate aerosol particles enhanced the formation of BSOA. In summer, the clean air mass originated from the ocean, and chlorine depletion was observed. We also found that concentrations of the total SOA tracers were correlated with HCl ($R^2 = 0.545$) and chlorine ions ($r = 0.280$–0.639) in $PM_{2.5}$, reflecting the contribution of Cl-initiated volatile organic compound (VOC) oxidations to the formation of SOA. In winter, the northeast dominant wind direction brought continental polluted air mass to the monitoring site, affecting the transformation of BSOA tracers. This implied that anthropogenic emissions, atmospheric oxidation capacity and halogen chemistry have significant effects on the formation of BSOA in the southeast coastal area.

Published by Copernicus Publications on behalf of the European Geosciences Union.

1 Introduction

Secondary organic aerosol (SOA) has attracted widespread scientific research concerns due to its potential impacts on climate change, human health and air quality (Shrivastava et al., 2017; Reid et al., 2018; Zhu et al., 2019; Wang et al., 2021b). Understanding the formation of SOA and assessing its relevance for environmental effects become an integral part of aerosol chemistry (Charan et al., 2019; Xiao et al., 2020; Palmer et al., 2022). However, due to its complex precursors and atmospheric physical or chemical processes, SOA prediction by air quality models remains highly uncertain (McFiggans et al., 2019). Therefore, it is necessary to better explore missed SOA sources and unknown SOA formation mechanisms.

SOA is produced by the conversion of biogenic and anthropogenic volatile organic compounds (BVOCs and AVOCs) through complex homogeneous and heterogeneous reactions (Charan et al., 2019; Xiao et al., 2020; Mahilang et al., 2021). BVOCs are the main precursors of SOA on a global scale, while AVOCs are the predominant contributors to SOA in urban areas (Hallquist et al., 2009; Wang et al., 2021a). Recently, laboratory, field and modeling studies have shown that anthropogenic emissions greatly affect the formation of biogenic secondary organic aerosol (BSOA) (Hoyle et al., 2011; Shrivastava et al., 2019; P. Zhang et al., 2019; Y. Q. Zhang et al., 2019; Mahilang et al., 2021; Xu et al., 2021). Anthropogenic air pollutants, such as NO_x, SO_2, NH_3 and aerosols, could influence the conversion of BVOCs to the particulate phase and the production of nitrogen and sulfur compounds (Wang et al., 2020). NO_x is one of the important drivers of SOA formation and yields during both day- and nighttime through alternating the fate of peroxy radicals (RO_2•) (Sarrafzadeh et al., 2016; Newland et al., 2021). While •OH dominates the photochemical oxidation of BVOC during daylight hours, NO_3• becomes one of the main oxidants for BSOA and organic nitrate formation at night. SO_2 also plays an important role in changing SOA formation from BVOC photooxidation and ozonolysis through sulfuric acid formation and acid-catalyzed heterogeneous reactions (Zhao et al., 2018; P. Zhang et al., 2019; Xu et al., 2021). In addition, NH_3 and amines can affect the SOA yields and composition through both gas-phase and heterogeneous reactions by reacting with sulfuric or nitric acid to generate secondary inorganic aerosols (SIA) (Ma et al., 2018; Liu et al., 2021; Lv et al., 2022). However, due to complex precursors and atmospheric processes, the combined effects of anthropogenic emissions and meteorological factors on the formation of SOA are not fully understood.

The coastal area of southeastern China is under the East Asian monsoon control, which causes an obvious alternation of polluted and clean air masses from continental and ocean area, respectively (Wu et al., 2019; Hong et al., 2021). Also, the local geographical environment, including relatively high humidity, dense vegetation and strong atmospheric oxidation capacity, provides a good chance to study the sources and formation mechanisms of SOA. In our previous studies, ground-based observations in a mountainous forest area of this region showed that BSOA tracers were the largest contributor to SOA, and the aerosols were highly oxidized (Hong et al., 2019). However, with the development of rapid urbanization, anthropogenic emissions will be of great significance on SOA formation (Liu et al., 2020). Halogen radicals (chlorine, bromine, iodine) have an important role in tropospheric oxidants chemistry and organic aerosol (OA) formation (X. Wang et al., 2021). Therefore, it is necessary to investigate the sources and formation mechanisms of SOA in coastal urban areas, so as to provide a scientific basis for the estimation of regional SOA budgets and $PM_{2.5}$ pollution control.

In this study, a continuous $PM_{2.5}$ sampling campaign with a 4 h time resolution was conducted in a coastal city of southeastern China during the winter and summer period. Seasonal, diurnal variations and secondary organic carbon (SOC) contributions of SOA tracers were analyzed. Atmospheric processes identified by SOA tracers in different seasons were further analyzed. Finally, the combined effects of anthropogenic emissions and major environmental factors on promoting SOA formation were discussed.

2 Materials and methods

2.1 Sample collection

The sampling was performed at the Institute of Urban Environment, Chinese Academy of Sciences (118.06° E, 24.61° N), which is located in a suburban area of Xiamen, a coastal city of southeastern China. Detailed information about the air monitoring supersite was described in our previous study (Hong et al., 2021). Briefly, time-resolved (00:00–08:00, 08:00–12:00, 12:00–16:00, 16:00–20:00, 20:00–24:00 CST – China standard time) $PM_{2.5}$ samples were collected on the rooftop of the station (about 70 m above the ground). The sampling was carried out using a high-volume (1.05 m^3 min^{-1}) sampler (TH-1000C, Wuhan Tianhong, China) with a $PM_{2.5}$ inlet from 10 to 18 January, and from 5 to 14 July 2020. All samples were collected onto prebaked (450 °C, 6 h) quartz fiber filters. Field blank samples were also collected. The sample filters were separately sealed in aluminum foil and stored in a freezer (−20 °C) prior to analysis.

2.2 SOA tracers analysis by GC–MS

The isoprene-derived SOA (SOA_I) tracers included two methyltetrols (MTLs: 2-methylthreitol (MTL1) and 2-methylerythritol (MTL2)), C5-alkene triols (cis-2-methyl-

1,3,4-trihydroxy-1-butene, trans-2-methyl-1,3,4-trihydroxy-1-butene, and 3-methyl-2,3,4-trihydroxy-1-butene) and 2-methylglyceric acid (MGA). The monoterpene-derived SOA (SOA_M) tracers were composed of pinic acid (PA), pinonic acid (PNA), 3-hydroxyglutaric acid (HGA), 3-methyl-1,2,3-butanetricarboxylic acid (MBTCA), 3-hydroxy-4,4-dimethylglutaric acid (HDMGA), and 3-acetylglutaric acid (AGA). The β-caryophyllene-derived SOA (SOA_C) tracer was β-caryophyllenic acid (CPA), the toluene-derived SOA (SOA_A) tracer was 2,3-dihydroxy-4-oxopentanoic acid (DHOPA) and levoglucosan (LEV) as a tracer of biomass burning. Due to the lack of authentic standards, surrogate standards (including erythritol, malic acid, PA and citramalic acid) were used to compensate for unavoidable assay variance of SOA_I, SOA_M, SOA_C and SOA_A tracers in each sample during the pretreatment process, respectively (Fu et al., 2009). However, inherent low volatility of isoprene SOA tracers could cause the uncertainties of using the gas chromatography–mass spectrometry (GC–MS) method, and low-volatility oligomers might break down into monomers, such as C5-alkene triols and 2-methyltetrols (Lopez-Hilfiker et al., 2016; Hu et al., 2016). Therefore, some uncertainty remained in quantifying the abundance of certain SOA tracers.

The analytical procedure of 15 SOA tracers was published in our previous studies (Hong et al., 2019; Liu et al., 2020). Briefly, the filter samples were ultrasonically extracted with a mixture of dichloromethane and methanol (2 : 1, v/v) three times for 10 min. The mixed extracts were filtered with a polytetrafluoroethylene (PTFE) filter (0.22 µm), dried with high purity N_2 (99.99 %), and then derivatized with 60 µL of N,O-bis-(trimethylsilyl) trifluoroacetamide (BSTFA) with 1 % trimethylsilyl chloride and 10 µL of pyridine at 70 °C for 3 h. At last, 140 µL of internal standard solution (^{13}C n-alkane solution, 1.507 ng µL^{-1}) was added into the samples. Then, relative response factors (RRFs) of surrogate and internal standard were calculated to quantify the targeted organic tracers in each sample. Details of SOA tracers' calculated concentrations based on RRFs were presented in our previous studies (Hong et al., 2019; Liu et al., 2020).

Fifteen SOA tracers were determined by gas chromatography–mass selective detector (GC–MSD) (7890A/5975C, Agilent Technologies, Inc., USA) with a DB-5 MS silica capillary column (i.d. 30 × 0.25 mm, 0.25 µm film thickness). A 1 µL sample was injected with splitless mode and high purity helium (99.999 %) was used as carrier gas at a stable flow of 1.0 mL min^{-1}. The GC temperature was initiated at 100 °C (held for 1 min) and then to 300 °C at 5 °C min^{-1}, and kept at 300 °C for 10 min. The operation mode is an electron ionization (EI) mode of 70 eV. The method detection limits (MDLs) for erythritol and PNA were 0.01 and 0.02 ng m^{-3}, respectively. The recoveries of erythritol, PNA, malic acid, PA and citramalic acid were 67 ± 2 %, 73 ± 1 %, 75 ± 1 %, 88 ± 7 % and 82 ± 8 %, respectively. SOA tracers were not detected in the field blank samples.

2.3 Observations in the air monitoring supersite

Water-soluble inorganic ions (WSII) in $PM_{2.5}$ (Cl^-, SO_4^{2-}, NO_3^-, Na^+, K^+, NH_4^+, Mg^{2+}, and Ca^{2+}) and gas pollutants (HCl, HONO, HNO_3, NH_3) were measured hourly using a monitoring device for aerosols and gases in ambient air (MARGA 2080; Metrohm Applikon B.V.; Delft, Netherlands). Internal calibration was carried out using LiBr standard solutions. The detection limit of Cl^-, SO_4^{2-}, NO_3^-, Na^+, K^+, NH_4^+, Mg^{2+}, and Ca^{2+} were 0.01, 0.04, 0.05, 0.05, 0.09, 0.05, 0.06 and 0.09 µg m^{-3}, respectively.

Hourly mass concentrations of $PM_{2.5}$ and PM_{10} were measured using a tapered element oscillating microbalance (TEOM1405, Thermo Scientific Corp., MA, USA). NO_2, SO_2, and O_3 were monitored using continuous gas analyzers (TEI 42i, 43i, and 49i, Thermo Scientific Corp., MA, USA). Ambient meteorological parameters including relative humidity (RH), temperature (T), wind speed (WS), and wind direction (WD) were obtained by an ultrasonic atmospherium (150WX, Airmar, the USA). Photolysis frequencies were determined using a photolysis spectrometer (PFS-100, Focused Photonics Inc., Hangzhou, China), including the photolysis rate constants J (O^1D), J (HCHO_M), J (HCHO_R), $J(NO_2)$, J (H_2O_2), J (HONO), J (NO_3_M) and J (NO_3_R), and the spectral band ranged from 270 to 790 nm. Boundary layer height (BLH) based on ERA-5 reanalysis dataset was downloaded from the following link: https://www.ecmwf.int/en/forecasts/datasets/reanalysis-datasets/era5 (last access: 14 December 2021).

2.4 Estimation of SOC using a tracer-based method

The fraction of SOC formed by the oxidation of monoterpene, isoprene, β-caryophyllene and toluene was estimated using a tracer-based method (Kleindienst et al., 2007; Hong et al., 2019). It is defined as $[SOC] = \sum i[tri]/f_{SOC}$, where [SOC] represents the mass concentration of SOC (µgC m^{-3}) and $\sum i$ [tri] means the sum of the concentration of individual SOA tracers (µg m^{-3}). The carbon mass fractions (f_{SOC}) of monoterpene, isoprene, β-caryophyllene and toluene were 0.231 ± 0.111, 0.155 ± 0.039, 0.023 ± 0.005 and 0.008 ± 0.003, respectively, based on smog-chamber experimental data (Kleindienst et al., 2007).

2.5 Aerosol acidity and OH calculation

The forward mode of the ISORROPIA II thermodynamic model was used to calculate the aerosol acidity (pH) (Fountoukis and Nenes, 2007). ISORROPIA II can calculate liquid water content (LWC), based on total SO_4^{2-}, NO_3^- (gas HNO_3 plus particle NO_3^-), Cl^-, ammonia gas (NH_3 plus particle NH_4^+), non-volatile cations (Na^+, K^+, Ca^{2+}, Mg^{2+}), and meteorological factors (RH and T) (Rumsey et al., 2014; Guo et al., 2016). The pH value from ISORROPIA II was

calculated using the following equation:

$$\mathrm{pH} = -\lg\left(\frac{1000 \times H^+}{\mathrm{LWC}}\right), \quad (1)$$

where H^+ is the hydronium ion concentration loading for an air sample ($\mu g\,m^{-3}$).

The OH concentration ([OH]) was estimated using the NO_2 and HONO concentrations and the photolysis rate constants (J) of NO_2, O_3, and HONO, according to the following improved empirical formula (Wen et al., 2019):

$$[\mathrm{OH}] = 4.1 \times 10^9 \times \frac{J(\mathrm{O^1D})^{0.83} \times J(\mathrm{NO_2})^{0.19} \times (140 \times \mathrm{NO_2} + 1) + \mathrm{HONO} \times J(\mathrm{HONO})}{0.41 \times \mathrm{NO_2^2} + 1.7 \times \mathrm{NO_2} + 1 + \mathrm{NO} \times k_{\mathrm{NO+OH}} + \mathrm{HONO} \times k_{\mathrm{HONO+OH}}} \quad (2)$$

2.6 Statistical analysis

Correlation analysis by SPSS 22.0 software (IBM, Armonk, NY, USA) was used to study the relationship among SOA tracers, meteorological parameters and criteria air pollutants. One-way analysis of variance (ANOVA) was adopted to examine the variations of different factors.

2.7 Backward trajectory analysis

Hybrid Single-Particle Lagrangian Integrated Trajectory (HYSPLIT) was used to analyze the impacts of air masses on Xiamen during different seasons. Backward trajectories of 72 h were calculated every hour at a height of 500 m. The meteorological data with a resolution of 1° longitude × 1° latitude were obtained from the NCEP/GDAS. Cluster analysis was adopted using the total spatial variance (TSV).

3 Results and discussion

3.1 Overview of air pollutants

The concentrations of criteria air pollutants, including SO_2, CO, NO_2, O_3, $PM_{2.5}$ and PM_{10}, and meteorological parameters during winter and summer are shown in Fig. 1. The concentrations of $PM_{2.5}$ in winter ranged from 14.9 to 75.3 $\mu g\,m^{-3}$ with an average of 42.1 $\mu g\,m^{-3}$, which was much higher than that (the average of 18.4 $\mu g\,m^{-3}$) in summer, ranging from 12.8 to 46.4 $\mu g\,m^{-3}$. The concentrations of CO, NO_2 and PM_{10} showed similar seasonal trends to the pattern of $PM_{2.5}$. In contrast, O_3 had the highest concentration in summer, which was attributed to the formation of photochemical reactions under strong UV radiation and the weak titration of nitrogen oxides. Meanwhile, the concentration of SO_2 ($8.37 \pm 0.79\ \mu g\,m^{-3}$) in summer was also higher than that ($2.63 \pm 1.95\ \mu g\,m^{-3}$) in winter, mainly attributed to the influence of coal combustion and ship emissions. The monitoring site was located approximately 15 km away from the Xiamen port area and a coal-fired power plant (4 × 300 kW) in the south. Southerly winds prevailed in summer, which might have caused the relatively high concentration of SO_2 in the monitoring site.

3.2 Temporal variations of SOA tracers and estimated SOC

Temporal variations of individual SOA tracers are shown in Fig. S1 in the Supplement. The average concentrations of total SOA tracers in winter and summer were 37.3 and 111.3 $ng\,m^{-3}$, respectively. The predominance of SOA_M (26.6 $ng\,m^{-3}$), followed by ASOA (4.60 $ng\,m^{-3}$), SOA_I (4.35 $ng\,m^{-3}$) and SOA_C (1.76 $ng\,m^{-3}$) was observed in winter while in summer, SOA_I (54.4 $ng\,m^{-3}$) and SOA_M (47.8 $ng\,m^{-3}$) were the main contributors to total SOA tracers, followed by ASOA (6.64 $ng\,m^{-3}$) and SOA_C (2.45 $ng\,m^{-3}$). In summer, BSOA tracers showed much higher concentrations in the daytime (149.3 $ng\,m^{-3}$) than at night (60.1 $ng\,m^{-3}$), while inverse results were observed in winter (30.4 and 35.0 $ng\,m^{-3}$ in the day- and nighttime, respectively). As shown in Table S2 in the Supplement, in summer, SOA_I ranged from 21.3 to 293.2 $ng\,m^{-3}$ (average of $82.0 \pm 66.2\ ng\,m^{-3}$) in the daytime and the concentrations of SOA_I ranging from 6.81 to 110.1 $ng\,m^{-3}$ (average of $26.8 \pm 24.6\ ng\,m^{-3}$) were observed at night. However, in winter, the concentrations of isoprene SOA tracers in the daytime, ranging from 1.36 to 11.1 $ng\,m^{-3}$ (average of $3.79 \pm 2.37\ ng\,m^{-3}$), were lower than those (average of $4.91 \pm 3.75\ ng\,m^{-3}$) in the nighttime. As shown in Fig. 2, diurnal variations of SOA_M, SOA_I, CPA and DHOPA tracers in summer showed high levels in the afternoon (12:00–16:00 CST), due to the impacts of beneficial photochemical oxidation conditions caused by high temperature and strong UV radiation. The related SOA tracers were consistent with the emissions of their precursors including BVOCs and AVOCs, similar to our previous studies (Hong et al., 2019; Liu et al., 2020). However, the SOA tracers in winter showed the lowest concentrations in the morning (08:00–12:00 CST), related to the favorable dispersion conditions caused by the increasing planetary BLH (Fig. 1). The LEV, a typical tracer of biomass burning, with a similar seasonal and diurnal trend to other tracers, was observed. However, LEV may not be as stable in the atmosphere, especially under high RH conditions (Hoffmann et al., 2010). In this study, it could be difficult to reflect the real concentration of LEV. A correlation of CPA with LEV was carried out (Fig. S2), just to discuss the impacts of biomass burning on the distribution of CPA tracers through local or long-range transport. Totally, high concentrations of BSOA tracers were found in the daytime and in summer, indicating the effects of temperature on BVOC emissions and their photochemical oxidations. The concentrations of BSOA tracers in winter increased in the nighttime, due to the changing nocturnal boundary layer.

As shown in Fig. S2a and b, SOA tracer-based SOC in winter and summer were estimated. The concentrations of SOC in summer were higher than those in winter, attributed

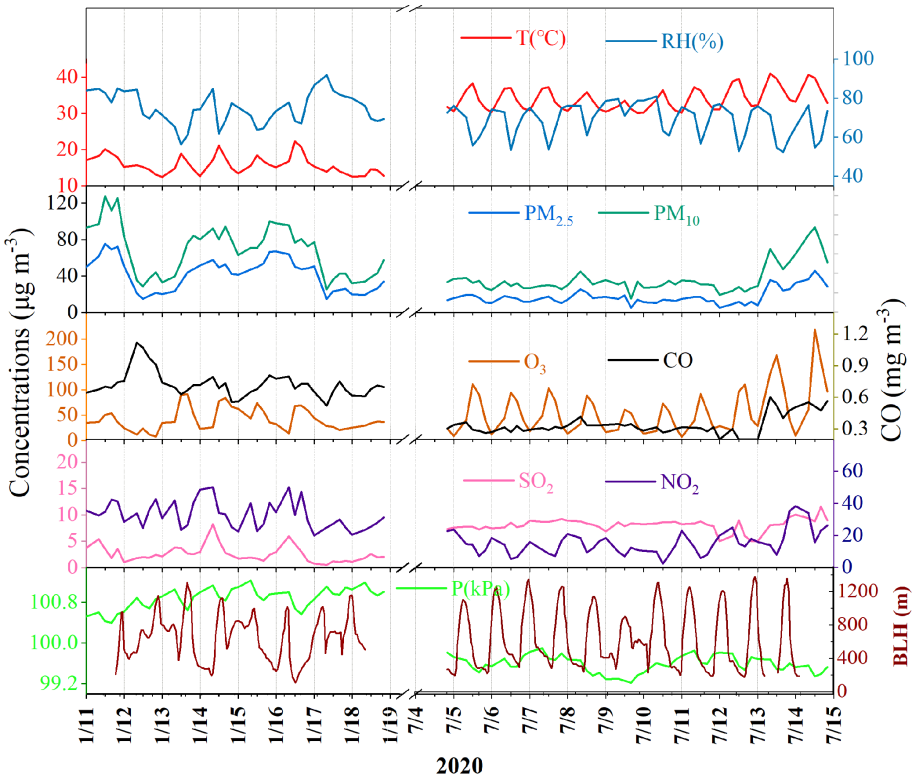

Figure 1. Time series of criteria air pollutants and meteorological parameters during the sampling period.

to the increase of flourishing vegetation emissions and photochemical reactions under high temperature and strong solar radiation conditions. For individual SOA tracers, the concentrations of monoterpene-derived SOC were comparable to the toluene-derived SOC, which were higher than isoprene-derived SOC and β-caryophyllene-derived SOC. An obvious trend of diurnal variations of isoprene-derived SOC in summer was observed, which was consistent with the diurnal pattern of isoprene concentration (Fig. S3). However, no similar trend was found in winter, attributed to the influence of low temperature on inhibiting the emissions of isoprene from various kinds of plants. In addition, the toluene-, monoterpene-, isoprene- and β-caryophyllene-derived SOC in summer accounted for 40.0 %, 39.2 %, 15.7 % and 5.1 % of the total SOC, respectively (Fig. S2c, d). However, in winter, the percentages of toluene-, monoterpene-, isoprene- and β-caryophyllene-derived SOC were 47.2 %, 42.1 %, 3.2 % and 7.6 %, respectively. The percentages of isoprene-derived SOC estimated from different precursors varied significantly among the seasons. High temperature enhanced the emissions of isoprene, and strong solar radiation favored the formation of isoprene SOA tracers, contributing to the highest isoprene-derived SOC percentage in summer (Ding et al., 2014). The highest percentages of toluene-derived SOC (47.2 %) in winter were related to anthropogenic emissions and adverse diffusion conditions.

3.3 Atmospheric process indication of BSOA tracers

As shown in Fig. 3, percentages of different types of SOA tracers in winter and summer were calculated. In summer, the monoterpene, isoprene, toluene and β-caryophyllene SOA tracers accounted for 45.8 %, 45.6 %, 6.2 % and 2.3 % of the total SOA tracers, respectively. However, in winter, the percentages of monoterpene, isoprene, toluene and β-caryophyllene SOA tracers were 70.1 %, 14.0 %, 11.0 % and 4.9 %, respectively. The percentage of SOA_I tracers decreased sharply due to the impacts of temperature on isoprene emissions, which was consistent with our previous findings (Hong et al., 2019). Meanwhile, the concentrations of SOA_M tracers were the largest in both seasons, due to a large amount of monoterpene emissions from the related plant species. Xiamen is an international garden city, which is located in the coastal area of southeastern China. Monoterpene, such as α/β-pinene, is mostly emitted by coniferous plants and most flowers and fruits, while isoprene originates from broad-leaved trees and deciduous plants (Ding et al., 2014; Shrivastava et al., 2017; Yang et al., 2021).

The first (PA and PNA) and later generation (HGA, AGA, HDMGA and MBTCA) products were used to evaluate the aging degree of SOA_M (Ding et al., 2014; Hong et al., 2019). In this study, HGA (32.2 %) was the major component of α/β-pinene tracers, followed by PA (30.5 %), PNA (21.8 %), HDMGA (7.3 %), MBTCA (6.8 %), and AGA (1.5 %). The

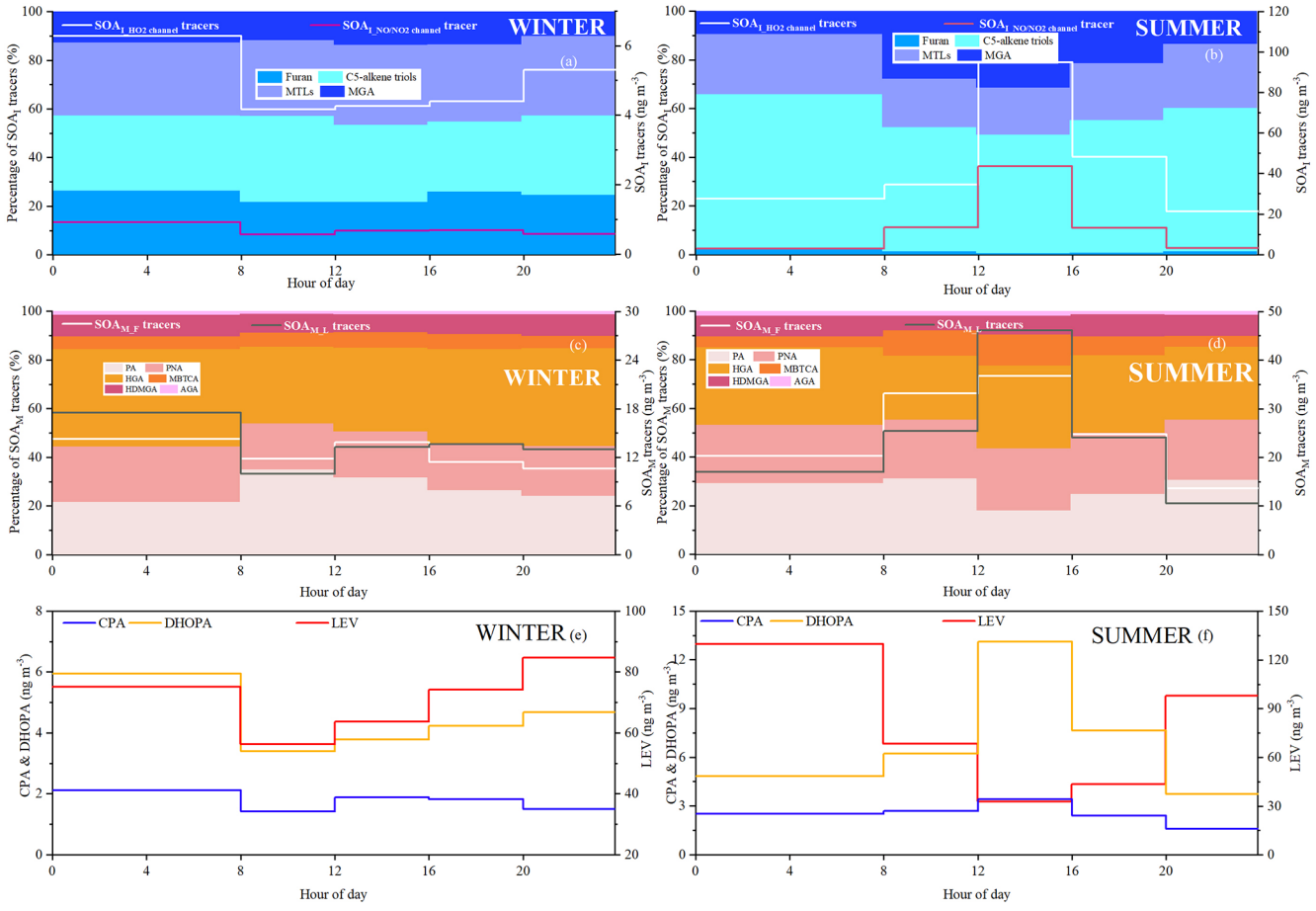

Figure 2. Diurnal variation of individual SOA tracers during winter **(a, c, e)** and summer **(b, d, f)**.

percentages of PA and PNA were much higher than those in mountainous background areas (PA: 9 % and PNA: 3 %) (Hong et al., 2019), suggesting the contribution of preliminary products to SOA in urban areas. As shown in Fig. 3, the percentages of PA and PNA in winter (21.8 % and 14.2 %) were higher than those in summer (14.2 % and 10.7 %). Reacting with atmospheric oxidants including O_3 and OH, PA and PNA were transformed into MBTCA (Offenberg et al., 2007). This is the reason why the proportions of PA and PNA had a significant decreasing trend from winter to summer. The ratio of MBTCA / (PA+PNA) in summer and winter were 0.16 ± 0.09 and 0.12 ± 0.07, respectively, which also proved the impacts of atmospheric oxidation capacity on the aging degree of SOA_M. In addition, the ratio of HGA / MBTCA could be used to distinguish the contribution of α-pinene or β-pinene to the SOA_M formation (Jaoui et al., 2005; Ding et al., 2014). Low ratio of HGA / MBTCA (~ 1.0) showed that α-pinene was the major precursor for SOA_M (Lewandowski et al., 2013). The ratio of HGA / MBTCA with an average of 5.78 in Xiamen was high, suggesting the contribution of β-pinene to SOA_M.

As shown in Fig. 3, MTLs and C5 alkene triols were the main components of the total SOA_I, with an average percentage of 68.0 ± 14.9 %, indicating a low-NO_x environment (Ding et al., 2014; Liu et al., 2020). In summer, the percentages of MTLs and C5 alkene triols to the total SOA tracers in summer (21.8 % and 14.2 %) were obviously higher than those in winter (4.2 % and 4.3 %). This was consistent with the fact that the concentrations of NO_2 ($14.8 \pm 7.46\,\mu g\,m^{-3}$) in summer were significantly lower than those ($32.7 \pm 32.6\,\mu g\,m^{-3}$) in winter. Previous studies found that MTLs and C5 alkene triols were formed by the OH and HO_2 radicals via the HO_2 channel under low-NO_x conditions (Surratt et al., 2010). C5 alkene triols are mainly produced by acid-catalyzed reactions of Isoprene Epoxydiols (IEPOX) in the gas phase, while MTLs are formed by ring-opening products of IEPOX (Surratt et al., 2007, 2010). The ozonolysis of isoprene was also an important pathway for MTLs in the presence of acid sulfate aerosols (Riva et al., 2016).

The typical tracer of sesquiterpenes, CPA, is formed by the photooxidation of β-caryophyllene (Jaoui et al., 2007). As shown in Fig. 3, CPA in winter and summer accounted for

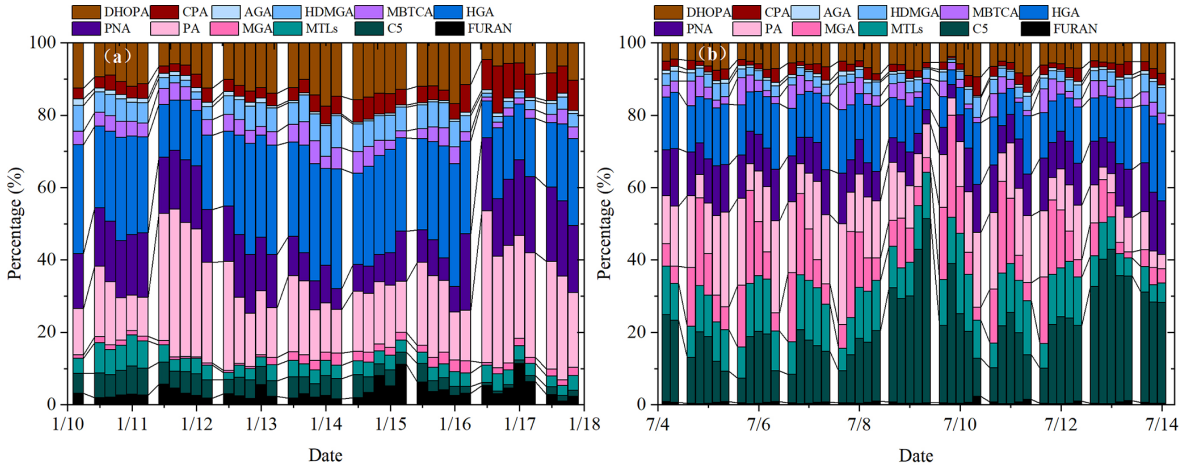

Figure 3. Percentages of isoprene, monoterpene, β-caryophyllene and toluene SOA tracers in winter **(a)** and summer **(b)**.

5.0 % and 2.3 % of the total SOA tracers, respectively. This is because the percentage of SOA_I has significant increases in summer. The concentrations of CPA ($2.5 \pm 2.0\,ng\,m^{-3}$) in summer were higher than that ($1.7 \pm 0.8\,ng\,m^{-3}$) in winter, probably attributed to the emissions of β-caryophyllene driven by temperature and solar radiation. The CPA has a good correlation with DHOPA in summer (Fig. S4), suggesting the influence of photochemical oxidation (Liu et al., 2020). However, the CPA was not correlated with LEV in both seasons, reflecting the limited contribution of biomass burning (Y.-Q. Zhang et al., 2019).

3.4 Impacts of aerosol acidity on BSOA formation

Aerosol acidity (pH) was an important factor in SOA formation (Surratt et al., 2007; Offenberg et al., 2009; P. Zhang et al., 2019; Y. Zhang et al., 2019). Time series of aerosol pH calculated by ISORROPIA II is shown in Fig. 4. The $PM_{2.5}$ in Xiamen was moderately acidic with a daily pH range from 3.68 to 4.67. The highest aerosol pH was observed in winter, and the lowest pH in summer. This is with similar seasonal trend, close to the Yangtze River Delta (YRD) region, but obviously lower levels than those in the North China Plain (NCP) cities of China (Zhou et al., 2021). In general, the aerosol pH in Chinese cities were higher than those in the United States and Europe.

A declining pH trend during the daytime was observed (Fig. 4), which was related to the changes of chemical compositions and environmental conditions. The aerosol pH levels ($\sim$ 3 to 6) were related to a shift from sulfate- to nitrate-dominated aerosols (Guo et al., 2017). According to the multiphase buffer theory, the peak buffer pH (pKa*) regulated the aerosol pH, and temperature could obviously cause the variation of aerosol pH (Zheng et al., 2020). To further discuss the impacts of aerosol pH on BSOA formation in a coastal city, we analyzed the relationship between BSOA tracers and seed particles with different pH and LWC (Fig. S5 and Table 1).

In Table 1, the BSOA tracers were linearly correlated with aerosol pH and SO_4^{2-}. In summer, BSOA tracers in the particle phase were found to increase with increasing acidity, which was attributed to the presence of acid-catalyzed aerosols. For example, isoprene SOA tracers are mainly formed through acid-catalyzed reactive uptake of isoprene-derived epoxydiols (IEPOX) onto sulfate aerosol particles. In our previous studies, we have reported that high concentrations of MTLs were related to sulfate, which could significantly promote the formation of isoprene-SOA tracers (Liu et al., 2020). Other studies also found that sulfate could increase the BSOA production by promoting acid-catalyzed ring-opening reactions (Xu et al., 2015). In contrast, positive correlations between BSOA tracers and aerosol pH in winter were observed, indicating that the formation of BSOA was predominantly enhanced by other factors, except for the aerosol pH. The aerosol pH in winter was higher than in summer, probably due to the influence of nitrate-dominated aerosols. Also, the aged aerosols through long-range transport might have resulted in the increase of BSOA tracers and aerosol pH.

In addition, positive correlation between BSOA tracers and LWC were observed (Table 1), probably attributed to the effects of LWC on determining the peak buffer pH (pKa*). Zheng et al. (2020) reported that the buffering effect of ammonia suppresses the contribution of different chemical compositions in aerosol particles, making LWC the primary determinant of aerosol pH. Other studies have demonstrated that the uptake coefficient of first-generation oxidation products, especially for carbonyl compounds, might depend on RH (Luo et al., 2019). Meanwhile, high LWC could reduce the aerosol particle viscosity, which is a benefit to the generation of the reactive intermediate such as IEPOX, or other oxidation products of VOC into an aqueous-phase of aerosol particles, thereby promoting the formation of BSOA (P. Zhang et al., 2019; Y. Zhang et al., 2019).

https://doi.org/10.5194/acp-22-7827-2022

Table 1. Correlations between individual BSOA tracers and environmental factors in winter and summer.

Season	SOA tracer	pH	LWC	HONO	$PM_{2.5}$	Cl^-	NO_3^-	SO_4^{2-}	NH_3	SO_2	NO_2	O_x	T	RH	UV
Winter ($n = 39$)	C5	0.584**	0.701**	0.534**	0.690**	0.569**	0.710**	0.663**	0.705**	0.308	0.353*	0.203	0.361*	0.140	0.200
	MTLs	0.590**	0.705**	0.431*	0.665**	0.639**	0.707**	0.651**	0.757**	0.185	0.229	0.098	0.353*	0.295	−0.068
	MGA	0.390*	0.707**	0.261	0.668**	0.081	0.758**	0.572**	0.284	0.172	0.123	0.374*	0.377*	−0.019	0.238
	PA	0.432*	0.403**	0.463**	0.407**	0.481*	0.416*	0.488*	0.440*	0.446*	0.241	−0.193	0.319*	−0.205	0.145
	PNA	0.489**	0.579**	0.311	0.459**	0.516**	0.573**	0.533**	0.543**	0.08	0.071	−0.101	0.121	0.337*	−0.122
	HGA	0.443*	0.829**	0.352*	0.834**	0.600**	0.847**	0.754**	0.641**	0.275	0.299	0.451**	0.451**	0.043	0.210
	MBTCA	0.433*	0.678**	0.447**	0.670**	0.435*	0.733**	0.589**	0.710**	0.327*	0.253	0.492**	0.552**	−0.158	0.317
	HDMGA	0.421*	0.876**	0.401*	0.867**	0.631**	0.884**	0.813**	0.643**	0.335*	0.321*	0.526**	0.485**	−0.049	0.327
	AGA	0.570**	0.575**	0.370*	0.488**	0.577**	0.566**	0.544**	0.731**	0.126	0.181	0.019	0.279	0.298	−0.122
	CPA	0.212	0.462**	−0.068	0.452**	0.483**	0.437*	0.419*	0.255	−0.15	−0.170	0.016	0.079	0.200	−0.144
Summer ($n = 50$)	C5	−0.495**	0.425**	0.160	0.622**	−0.340*	0.268	0.625**	0.436**	0.254	0.025	0.649**	0.573**	−0.529**	0.247
	MTLs	−0.551**	0.131	0.055	0.272	−0.439**	0.131	0.428**	0.304*	0.089	−0.278	0.550**	0.610**	−0.594**	0.263
	MGA	−0.540**	0.029	0.116	0.132	−0.403**	0.066	0.472**	0.270	0.096	−0.410**	0.443**	0.633**	−0.668**	0.382*
	PA	−0.633**	0.483**	0.601**	0.461**	−0.135	0.541**	0.502**	0.405*	0.037	0.238	0.456**	0.626**	−0.558**	0.400*
	PNA	−0.664**	0.616**	0.387**	0.812**	−0.389**	0.450**	0.784**	0.503**	0.269	0.294*	0.769**	0.718**	−0.631**	0.404*
	HGA	−0.607**	0.612**	0.299*	0.836**	−0.384**	0.447**	0.770**	0.539**	0.316*	0.272	0.808**	0.670**	−0.599**	0.322
	MBTCA	−0.752**	0.415**	0.237	0.577**	−0.382**	0.359*	0.636**	0.501**	0.201	−0.052	0.712**	0.852**	−0.816**	0.588**
	HDMGA	−0.525**	0.618**	0.299*	0.833**	−0.342*	0.408**	0.768**	0.488**	0.358*	0.365**	0.746**	0.574**	−0.500**	0.240
	AGA	−0.684**	0.592**	0.447**	0.766**	−0.334*	0.479**	0.735**	0.435**	0.244	0.271	0.694**	0.720**	−0.634**	0.477**
	CPA	−0.552**	0.625**	0.441**	0.780**	−0.280*	0.453**	0.763**	0.307*	0.299*	0.503**	0.611**	0.529**	−0.458**	0.305

*/** Correlation coefficients with an asterisk indicate statistically significant relationships at $p = 0.05$, and two asterisks mean significant relationships at $p = 0.01$.

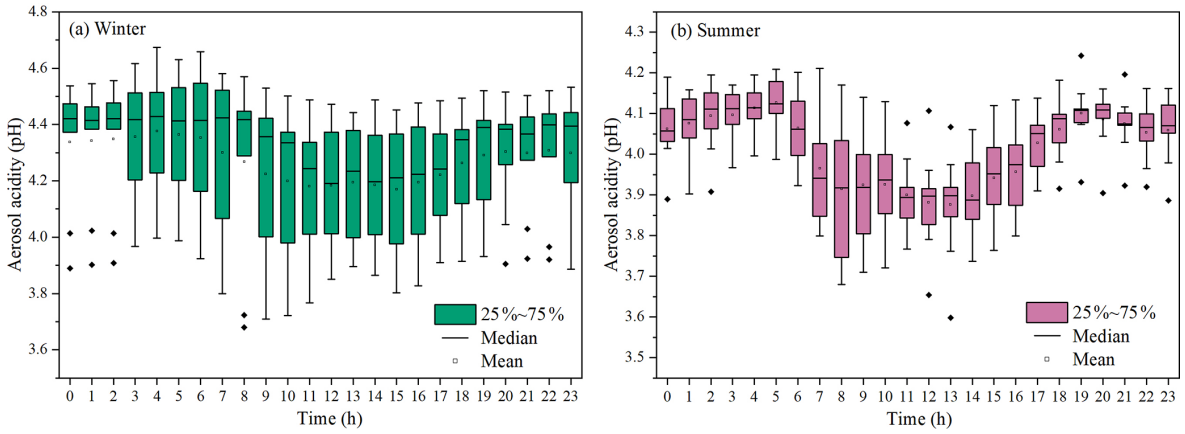

Figure 4. Diurnal variations of aerosol acidity (pH) during the wintertime **(a)** and summertime **(b)** period. (The boxes with error bars represent the 10th, 25th, 75th, and 90th percentiles.)

3.5 Impacts of chlorine on BSOA formation

Halogen radicals (Cl, Br and I) originated from sea salt aerosol (SSA) and have an important role in tropospheric oxidants chemistry (X. Wang et al., 2021). In this study, chlorine depletion was frequently observed in summer (Fig. 5b), indicating that HCl can be formed through acid (such as H_2SO_4 and HNO_3) displacement of SSA Cl^-. Moreover, concentrations of the total SOA tracers were positively correlated with HCl (Fig. 5a), suggesting the enhancement of SOA precursor transformation. Previous studies have found that Cl-initiated VOC oxidations could contribute to the formation of SOA (Wang and Ruiz, 2017; Dhulipala et al., 2019).

Under ammonia-rich conditions, HCl partitioned into the aqueous particulate phase mostly took place, and chlorine ions could affect aqueous oxidation of secondary organic compounds (Xu et al., 2021). As shown in Table 1, most of the SOA tracers in winter were correlated with the concentrations of chlorine ions in $PM_{2.5}$, while inverse results were observed in summer. In winter, the dominant wind direction is northeast (Fig. 6), and chlorine mainly came from continental polluted air mass, such as industrial and combustion emissions. So, anthropogenic pollutants through long-range transport might cause the enhancement of SOA tracer concentrations at the monitoring site. However, in summer, negative correlations of BSOA tracers and chlorine ions in $PM_{2.5}$ were found, probably due to the influence of chlorine depletion. As shown in Fig. 6, the dominant wind direction is southerly, and chlorine mainly originated from the spray of sea salt.

3.6 Enhanced formation of BSOA by anthropogenic emissions

Recent studies have indicated that anthropogenic emissions might affect SOA formation through multiple chemical processes, based on laboratory studies and field observations (Kari et al., 2019; Shrivastava et al., 2019; Y.-Q. Zhang et al., 2019; Cheng et al., 2021; Xu et al., 2021). In this study, we conducted the correlation analysis of individual SOA tracers and O_x ($= O_3+NO_2$), HONO, OH, SO_2, NH_3, $PM_{2.5}$, sulfate, nitrate, as well as meteorological parameters (including T, RH and UV) (Table 1).

Most of the SOA tracers have a significant positive correlation with NH_3, suggesting an enhancement effect on the formation of SOA (Table 1). NH_3 could affect the SOA yields through both gas-phase and heterogeneous reactions (Na et al., 2007; Ma et al., 2018; Hao et al., 2020). Gas-phase reactions between NH_3 and organic acids (such as PA and PNA) produced ammonium salts in the particle phase, which contributed to the increased SOA formation. However, not all gas-phase organic acids (e.g., MGA and pyruvic acid) could demonstrate gas-to-particle conversion (Na et al., 2007). When SOA formation had ceased, the addition of excessive NH_3 would result in the rapid decomposition of the main SOA species, due to the nucleophilic attack of NH_3 (Ma et al., 2018).

As an indicator of atmospheric oxidation capacity, the tropospheric odd oxygen O_x (O_3+NO_2) was calculated. As shown in Table 1, the majority of SOA tracers in summer showed significant positive correlations with O_x ($R > 0.5$, $P < 0.001$). However, in winter, a part of SOA_M tracers (e.g., HGA, MBTCA and HDMGA) were found to be significantly correlated with O_x. In addition, HONO and OH radicals, another critical indicator of atmospheric oxidation capacity, were also discussed. In this study, the concentration of OH radicals calculated from HONO in summer was higher than those in winter. In summer, the SOA_I tracers were correlated

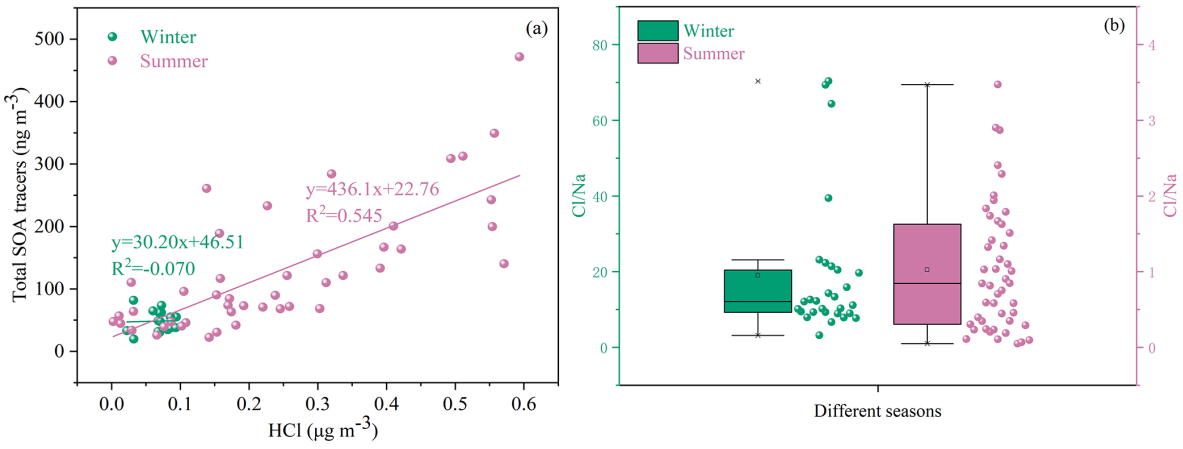

Figure 5. Correlations of total SOA tracers and HCl **(a)** and chlorine depletion **(b)** in different seasons.

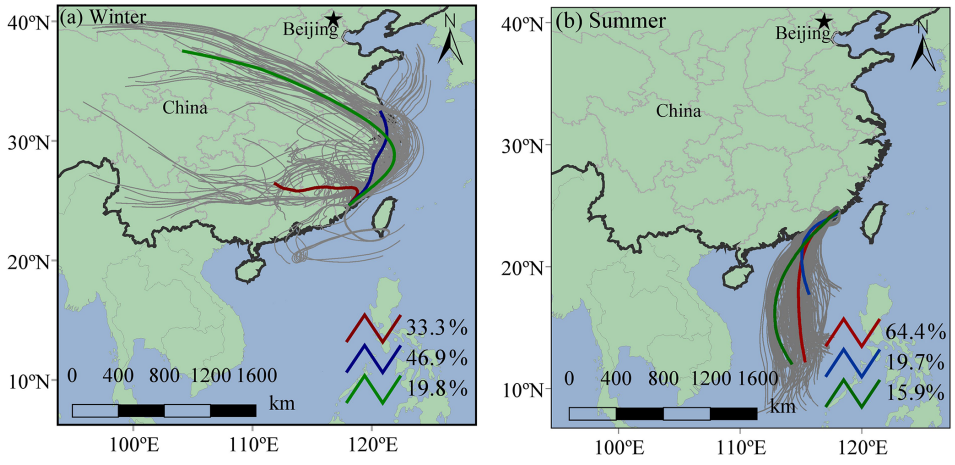

Figure 6. Backward trajectories analyses during the winter **(a)** and summer **(b)**.

with OH radicals (Fig. 7b), consistent with previous findings that OH radicals could promote the formation of SOA (Sarrafzadeh et al., 2016; Liu et al., 2019; Song et al., 2019; J. Zhang et al., 2019). Due to its photolysis to produce OH radicals during the daytime, HONO could facilitate SOA formation. In winter, the concentrations of SOA_I, SOA_M and ASOA tracers were correlated with HONO (Fig. 7a). These results indicated high concentrations of HONO and sufficient UV radiation could enhance the photochemical reactions of VOCs, which is consistent with our previous results on the formation of peroxyacetyl nitrate (PAN) (Hu et al., 2020). As for T and UV, it exhibited significantly positive correlations with the related SOA tracers, especially in summer. These results suggested that SOA tracers were produced from the photooxidation of VOC precursors (Cheng et al., 2021).

In addition, the SOA tracers were significantly positively correlated with $PM_{2.5}$ and its components, including NO_3^- and SO_4^{2-}. In the coastal cities of southeastern China, with the development of rapid urbanization, air pollution caused by motor vehicles and industrial emissions is becoming more frequent in winter (Wu et al., 2020). The Xiamen port is one of the top 10 ports in China, resulting from the impacts of ship emissions and port activities on ambient air quality (Xu et al., 2018), and the number of motor vehicles increased sharply in recent years. We also found that the 90th percentile of maximum daily average 8 h (MDA8) O_3 concentrations in Xiamen has increased significantly from 2015 to 2020 (Fig. S6). During the past several years, the elevated secondary inorganic components, including NO_3^-, SO_4^{2-} and NH_4^+, accounted for 40 %–50 % of the total $PM_{2.5}$, and organic matter (OM) ranged from 30 % to 40 % (Wu et al., 2019; Hong et al., 2021). These results also implied the effects of anthropogenic emissions and enhanced atmospheric oxidation capacity on the secondary formation of aerosol particles under atmospheric stagnant conditions.

4 Conclusions

Pollution characteristics and source identification of BSOA tracers during summer and winter in coastal areas of south-

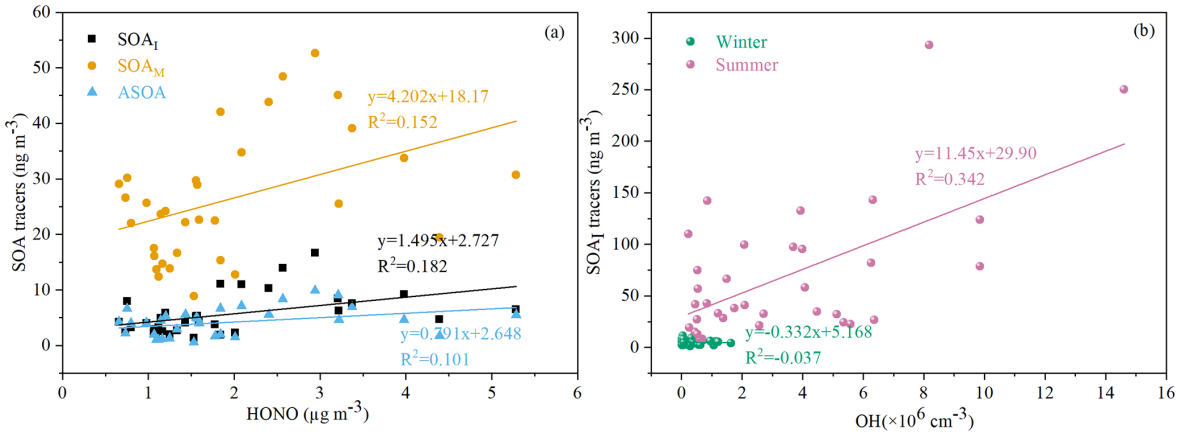

Figure 7. Relationship of SOA tracers and HONO **(a)** and its estimated OH **(b)**.

eastern China were investigated. The average concentration of total BSOA tracers in summer was higher than that in winter, with the predominance of SOA_M, followed by SOA_I and SOA_C. The BSOA tracers in summer were predominantly produced by the influence of photochemical oxidation under relatively clean conditions. However, in winter, the formation of BSOA tracers were attributed to the impacts of anthropogenic emissions and atmospheric stagnant conditions. In addition, the results also indicated that acid-catalyzed reactive uptake onto sulfate aerosol particles enhanced the formation of BSOA in both seasons. We further found that Cl-initiated VOC oxidations potentially accelerated the transformation of BSOA precursors through SSA originating from the ocean in summer and anthropogenic emissions in winter. This study demonstrated the combined effects of anthropogenic pollutants and atmospheric oxidation capacity on the formation of BSOA in coastal area.

Data availability. The data set related to this work can be accessed via https://doi.org/10.5281/zenodo.6376025 (Hong, 2022). The details are also available upon request from the corresponding author (ywhong@iue.ac.cn).

Supplement. The supplement related to this article is available online at: https://doi.org/10.5194/acp-22-7827-2022-supplement.

Author contributions. YH and XX contributed equally to this work. YH designed and wrote the manuscript. XX collected the data and contributed to the data analysis. DL, TL, XJ and KX performed modeling analyses and data analysis. JC supported funding of observation and research. ChunyL, TW and ChunsL contributed to revise the manuscript.

Competing interests. The contact author has declared that neither they nor their co-authors have any competing interests.

Disclaimer. Publisher's note: Copernicus Publications remains neutral with regard to jurisdictional claims in published maps and institutional affiliations.

Acknowledgements. The authors gratefully acknowledge Yanting Chen, Han Zhang and Xu Liao (Institute of Urban Environment, Chinese Academy of Sciences) for the guidance and assistance during sample pretreatment, and Lingling Xu and Mengren Li (Institute of Urban Environment, Chinese Academy of Sciences) for the discussion of this paper. This study was supported by Fujian Key Laboratory of Atmospheric Ozone Pollution Prevention and Xiamen Atmospheric Environment Observation and Research Station of Fujian Province (Institute of Urban Environment, Chinese Academy of Sciences).

Financial support. This research was financially supported by the foreign cooperation project of Fujian Province (grant no. 2020I0038), the Xiamen Youth Innovation Fund Project (grant no. 3502Z20206094), the Cultivating Project of Strategic Priority Research Program of Chinese Academy of Sciences (grant no. XDPB1903), the National Key Research and Development Program (grant no. 2016YFC0112200), State Key Laboratory of Environmental Chemistry and Ecotoxicology, Research Center for Eco-Environmental Sciences, CAS (grant no. KF2020-06), the FJIRSM&IUE Joint Research Fund (grant no. RHZX-2019-006) and the Center for Excellence in Regional Atmospheric Environment project (grant no. E0L1B20201).

Review statement. This paper was edited by Jason Surratt and reviewed by three anonymous referees.

References

Charan, S. M., Huang, Y., and Seinfeld, J. H.: Computational Simulation of Secondary Organic Aerosol Formation in Laboratory Chambers, Chem. Rev., 119, 11912–11944, https://doi.org/10.1021/acs.chemrev.9b00358, 2019.

Cheng, Y., Ma, Y., and Hu, D.: Tracer-based source apportioning of atmospheric organic carbon and the influence of anthropogenic emissions on secondary organic aerosol formation in Hong Kong, Atmos. Chem. Phys., 21, 10589–10608, https://doi.org/10.5194/acp-21-10589-2021, 2021.

Dhulipala, S. V., Bhandari, S., and Hildebrandt Ruiz, L.: Formation of oxidized organic compounds from Cl-initiated oxidation of toluene, Atmos. Environ., 199, 265–273, https://doi.org/10.1016/j.atmosenv.2018.11.002, 2019.

Ding, X., He, Q.-F., Shen, R.-Q., Yu, Q.-Q., and Wang, X.-M.: Spatial distributions of secondary organic aerosols from isoprene, monoterpenes, beta-caryophyllene, and aromatics over China during summer, J. Geophys. Res.-Atmos., 119, 11877–11891, https://doi.org/10.1002/2014jd021748, 2014.

Fountoukis, C. and Nenes, A.: ISORROPIA II: a computationally efficient thermodynamic equilibrium model for K^+–Ca^{2+}–Mg^{2+}–NH_4^+–Na^+–SO_4^{2-}–NO_3^-–Cl^-–H_2O aerosols, Atmos. Chem. Phys., 7, 4639–4659, https://doi.org/10.5194/acp-7-4639-2007, 2007.

Fu, P., Kawamura, K., Chen, J., and Barrie, L. A.: Isoprene, Monoterpene, and Sesquiterpene Oxidation Products in the High Arctic Aerosols during Late Winter to Early Summer, Environ. Sci. Technol., 43, 4022–4028, https://doi.org/10.1021/es803669a, 2009.

Guo, H., Sullivan, A. P., Campuzano-Jost, P., Schroder, J. C., Lopez-Hilfiker, F. D., Dibb, J. E., Jimenez, J. L., Thornton, J. A., Brown, S. S., Nenes, A., and Weber, R. J.: Fine particle pH and the partitioning of nitric acid during winter in the northeastern United States, J. Geophys. Res.-Atmos., 121, 10355–310376, https://doi.org/10.1002/2016JD025311, 2016.

Guo, H., Weber, R. J., and Nenes, A.: High levels of ammonia do not raise fine particle pH sufficiently to yield nitrogen oxide-dominated sulfate production, Sci. Rep., 7, 12109, https://doi.org/10.1038/s41598-017-11704-0, 2017.

Hallquist, M., Wenger, J. C., Baltensperger, U., Rudich, Y., Simpson, D., Claeys, M., Dommen, J., Donahue, N. M., George, C., Goldstein, A. H., Hamilton, J. F., Herrmann, H., Hoffmann, T., Iinuma, Y., Jang, M., Jenkin, M. E., Jimenez, J. L., Kiendler-Scharr, A., Maenhaut, W., McFiggans, G., Mentel, Th. F., Monod, A., Prévôt, A. S. H., Seinfeld, J. H., Surratt, J. D., Szmigielski, R., and Wildt, J.: The formation, properties and impact of secondary organic aerosol: current and emerging issues, Atmos. Chem. Phys., 9, 5155–5236, https://doi.org/10.5194/acp-9-5155-2009, 2009.

Hao, L., Kari, E., Leskinen, A., Worsnop, D. R., and Virtanen, A.: Direct contribution of ammonia to α-pinene secondary organic aerosol formation, Atmos. Chem. Phys., 20, 14393–14405, https://doi.org/10.5194/acp-20-14393-2020, 2020.

Hoffmann, D., Tilgner, A., Iinuma, Y., and Herrmann, H.: Atmospheric Stability of Levoglucosan: A Detailed Laboratory and Modeling Study, Environ. Sci. Technol., 44, 694–699, https://doi.org/10.1021/es902476f, 2010.

Hong, Y.: Dataset for ACP by Hong et al., 2022, Zenodo [data set], https://doi.org/10.5281/zenodo.6376025, 2022.

Hong, Y., Xu, X., Liao, D., Zheng, R., Ji, X., Chen, Y., Xu, L., Li, M., Wang, H., Xiao, H., Choi, S.-D., and Chen, J.: Source apportionment of $PM_{2.5}$ and sulfate formation during the COVID-19 lockdown in a coastal city of southeast China, Environ. Pollut., 286, 117577, https://doi.org/10.1016/j.envpol.2021.117577, 2021.

Hong, Z., Zhang, H., Zhang, Y., Xu, L., Liu, T., Xiao, H., Hong, Y., Chen, J., Li, M., Deng, J., Wu, X., Hu, B., and Chen, X.: Secondary organic aerosol of $PM_{2.5}$ in a mountainous forest area in southeastern China: Molecular compositions and tracers implication, Sci. Total Environ., 653, 496–503, https://doi.org/10.1016/j.scitotenv.2018.10.370, 2019.

Hoyle, C. R., Boy, M., Donahue, N. M., Fry, J. L., Glasius, M., Guenther, A., Hallar, A. G., Huff Hartz, K., Petters, M. D., Petäjä, T., Rosenoern, T., and Sullivan, A. P.: A review of the anthropogenic influence on biogenic secondary organic aerosol, Atmos. Chem. Phys., 11, 321–343, https://doi.org/10.5194/acp-11-321-2011, 2011.

Hu, B., Liu, T., Hong, Y., Xu, L., Li, M., Wu, X., Wang, H., Chen, J., and Chen, J.: Characteristics of peroxyacetyl nitrate (PAN) in a coastal city of southeastern China: Photochemical mechanism and pollution process, Sci. Total Environ., 719, 137493, https://doi.org/10.1016/j.scitotenv.2020.137493, 2020.

Hu, W., Palm, B. B., Day, D. A., Campuzano-Jost, P., Krechmer, J. E., Peng, Z., de Sá, S. S., Martin, S. T., Alexander, M. L., Baumann, K., Hacker, L., Kiendler-Scharr, A., Koss, A. R., de Gouw, J. A., Goldstein, A. H., Seco, R., Sjostedt, S. J., Park, J.-H., Guenther, A. B., Kim, S., Canonaco, F., Prévôt, A. S. H., Brune, W. H., and Jimenez, J. L.: Volatility and lifetime against OH heterogeneous reaction of ambient isoprene-epoxydiols-derived secondary organic aerosol (IEPOX-SOA), Atmos. Chem. Phys., 16, 11563–11580, https://doi.org/10.5194/acp-16-11563-2016, 2016.

Jaoui, M., Kleindienst, T. E., Lewandowski, M., Offenberg, J. H., and Edney, E. O.: Identification and quantification of aerosol polar oxygenated compounds bearing carboxylic or hydroxyl groups. 2. Organic tracer compounds from monoterpenes, Environ. Sci. Technol., 39, 5661–5673, https://doi.org/10.1021/es048111b, 2005.

Jaoui, M., Lewandowski, M., Kleindienst, T. E., Offenberg, J. H., and Edney, E. O.: β-caryophyllinic acid: An atmospheric tracer for β-caryophyllene secondary organic aerosol, Geophys. Res. Lett., 34, L05816, https://doi.org/10.1029/2006gl028827, 2007.

Kari, E., Hao, L., Ylisirniö, A., Buchholz, A., Leskinen, A., Yli-Pirilä, P., Nuutinen, I., Kuuspalo, K., Jokiniemi, J., Faiola, C. L., Schobesberger, S., and Virtanen, A.: Potential dual effect of anthropogenic emissions on the formation of biogenic secondary organic aerosol (BSOA), Atmos. Chem. Phys., 19, 15651–15671, https://doi.org/10.5194/acp-19-15651-2019, 2019.

Kleindienst, T. E., Jaoui, M., Lewandowski, M., Offenberg, J. H., Lewis, C. W., Bhave, P. V., and Edney, E. O.: Estimates of the contributions of biogenic and anthropogenic hydrocarbons to secondary organic aerosol at a southeastern US location, Atmos. Environ., 41, 8288–8300, https://doi.org/10.1016/j.atmosenv.2007.06.045, 2007.

Lewandowski, M., Piletic, I. R., Kleindienst, T. E., Offenberg, J. H., Beaver, M. R., Jaoui, M., Docherty, K. S.,

and Edney, E. O.: Secondary organic aerosol characterisation at field sites across the United States during the spring-summer period, Int. J. Environ. An. Ch., 93, 1084–1103, https://doi.org/10.1080/03067319.2013.803545, 2013.

Liu, S., Tsona, N. T., Zhang, Q., Jia, L., Xu, Y., and Du, L.: Influence of relative humidity on cyclohexene SOA formation from OH photooxidation, Chemosphere, 231, 478–486, https://doi.org/10.1016/j.chemosphere.2019.05.131, 2019.

Liu, S., Huang, D., Wang, Y., Zhang, S., Liu, X., Wu, C., Du, W., and Wang, G.: Synergetic effects of NH_3 and NO_x on the production and optical absorption of secondary organic aerosol formation from toluene photooxidation, Atmos. Chem. Phys., 21, 17759–17773, https://doi.org/10.5194/acp-21-17759-2021, 2021.

Liu, T., Hu, B., Xu, X., Hong, Y., Zhang, Y., Wu, X., Xu, L., Li, M., Chen, Y., Chen, X., and Chen, J.: Characteristics of $PM_{2.5}$-bound secondary organic aerosol tracers in a coastal city in Southeastern China: Seasonal patterns and pollution identification, Atmos. Environ., 237, 117710, https://doi.org/10.1016/j.atmosenv.2020.117710, 2020.

Lopez-Hilfiker, F. D., Mohr, C., D'Ambro, E. L., Lutz, A., Riedel, T. P., Gaston, C. J., Iyer, S., Zhang, Z., Gold, A., Surratt, J. D., Lee, B. H., Kurten, T., Hu, W. W., Jimenez, J., Hallquist, M., and Thornton, J. A.: Molecular Composition and Volatility of Organic Aerosol in the Southeastern US: Implications for IEPDX Derived SOA, Environ. Sci. Technol., 50, 2200–2209, https://doi.org/10.1021/acs.est.5b04769, 2016.

Luo, H., Jia, L., Wan, Q., An, T., and Wang, Y.: Role of liquid water in the formation of O-3 and SOA particles from 1,2,3-trimethylbenzene, Atmos. Environ., 217, 116955, https://doi.org/10.1016/j.atmosenv.2019.116955, 2019.

Lv, S., Wang, F., Wu, C., Chen, Y., Liu, S., Zhang, S., Li, D., Du, W., Zhang, F., Wang, H., Huang, C., Fu, Q., Duan, Y., and Wang, G.: Gas-to-Aerosol Phase Partitioning of Atmospheric Water-Soluble Organic Compounds at a Rural Site in China: An Enhancing Effect of NH_3 on SOA Formation, Environ. Sci. Technol., 56, 3915–3924, https://doi.org/10.1021/acs.est.1c06855, 2022.

Ma, Q., Lin, X. X., Yang, C. G., Long, B., Gai, Y. B., and Zhang, W. J.: The influences of ammonia on aerosol formation in the ozonolysis of styrene: roles of Criegee intermediate reactions, Roy. Soc. Open Sci., 5, 172171, https://doi.org/10.1098/rsos.172171, 2018.

Mahilang, M., Deb, M. K., and Pervez, S.: Biogenic secondary organic aerosols: A review on formation mechanism, analytical challenges and environmental impacts, Chemosphere, 262, 127771, https://doi.org/10.1016/j.chemosphere.2020.127771, 2021.

McFiggans, G., Mentel, T. F., Wildt, J., Pullinen, I., Kang, S., Kleist, E., Schmitt, S., Springer, M., Tillmann, R., Wu, C., Zhao, D. F., Hallquist, M., Faxon, C., Le Breton, M., Hallquist, A. M., Simpson, D., Bergstrom, R., Jenkin, M. E., Ehn, M., Thornton, J. A., Alfarra, M. R., Bannan, T. J., Percival, C. J., Priestley, M., Topping, D., and Kiendler-Scharr, A.: Secondary organic aerosol reduced by mixture of atmospheric vapours, Nature, 565, 587–593, https://doi.org/10.1038/s41586-018-0871-y, 2019.

Na, K., Song, C., Switzer, C., and Cocker, D. R.: Effect of Ammonia on Secondary Organic Aerosol Formation from α-Pinene Ozonolysis in Dry and Humid Conditions, Environ. Sci. Technol., 41, 6096–6102, https://doi.org/10.1021/es061956y, 2007.

Newland, M. J., Bryant, D. J., Dunmore, R. E., Bannan, T. J., Acton, W. J. F., Langford, B., Hopkins, J. R., Squires, F. A., Dixon, W., Drysdale, W. S., Ivatt, P. D., Evans, M. J., Edwards, P. M., Whalley, L. K., Heard, D. E., Slater, E. J., Woodward-Massey, R., Ye, C., Mehra, A., Worrall, S. D., Bacak, A., Coe, H., Percival, C. J., Hewitt, C. N., Lee, J. D., Cui, T., Surratt, J. D., Wang, X., Lewis, A. C., Rickard, A. R., and Hamilton, J. F.: Low-NO atmospheric oxidation pathways in a polluted megacity, Atmos. Chem. Phys., 21, 1613–1625, https://doi.org/10.5194/acp-21-1613-2021, 2021.

Offenberg, J. H., Lewis, C. W., Lewandowski, M., Jaoui, M., Kleindienst, T. E., and Edney, E. O.: Contributions of toluene and alpha-pinene to SOA formed in an irradiated toluene/alpha-pinene/NO_x/air mixture: Comparison of results using C-14 content and SOA organic tracer methods, Environ. Sci. Technol., 41, 3972–3976, https://doi.org/10.1021/es070089+, 2007.

Offenberg, J. H., Lewandowski, M., Edney, E. O., Kleindienst, T. E., and Jaoui, M.: Influence of Aerosol Acidity on the Formation of Secondary Organic Aerosol from Biogenic Precursor Hydrocarbons, Environ. Sci. Technol., 43, 7742–7747, https://doi.org/10.1021/es901538e, 2009.

Palmer, P. I., Marvin, M. R., Siddans, R., Kerridge, B. J., and Moore, D. P.: Nocturnal survival of isoprene linked to formation of upper tropospheric organic aerosol, Science, 375, 562–566, https://doi.org/10.1126/science.abg4506, 2022.

Reid, J. P., Bertram, A. K., Topping, D. O., Laskin, A., Martin, S. T., Petters, M. D., Pope, F. D., and Rovelli, G.: The viscosity of atmospherically relevant organic particles, Nat. Commun., 9, 956, https://doi.org/10.1038/s41467-018-03027-z, 2018.

Riva, M., Budisulistiorini, S. H., Zhang, Z., Gold, A., and Surratt, J. D.: Chemical characterization of secondary organic aerosol constituents from isoprene ozonolysis in the presence of acidic aerosol, Atmos. Environ., 130, 5–13, https://doi.org/10.1016/j.atmosenv.2015.06.027, 2016.

Rumsey, I. C., Cowen, K. A., Walker, J. T., Kelly, T. J., Hanft, E. A., Mishoe, K., Rogers, C., Proost, R., Beachley, G. M., Lear, G., Frelink, T., and Otjes, R. P.: An assessment of the performance of the Monitor for AeRosols and GAses in ambient air (MARGA): a semi-continuous method for soluble compounds, Atmos. Chem. Phys., 14, 5639–5658, https://doi.org/10.5194/acp-14-5639-2014, 2014.

Sarrafzadeh, M., Wildt, J., Pullinen, I., Springer, M., Kleist, E., Tillmann, R., Schmitt, S. H., Wu, C., Mentel, T. F., Zhao, D., Hastie, D. R., and Kiendler-Scharr, A.: Impact of NO_x and OH on secondary organic aerosol formation from β-pinene photooxidation, Atmos. Chem. Phys., 16, 11237–11248, https://doi.org/10.5194/acp-16-11237-2016, 2016.

Shrivastava, M., Cappa, C. D., Fan, J., Goldstein, A. H., Guenther, A. B., Jimenez, J. L., Kuang, C., Laskin, A., Martin, S. T., Ng, N. L., Petaja, T., Pierce, J. R., Rasch, P. J., Roldin, P., Seinfeld, J. H., Shilling, J., Smith, J. N., Thornton, J. A., Volkamer, R., Wang, J., Worsnop, D. R., Zaveri, R. A., Zelenyuk, A., and Zhang, Q.: Recent advances in understanding secondary organic aerosol: Implications for global climate forcing, Rev. Geophys., 55, 509–559, https://doi.org/10.1002/2016rg000540, 2017.

Shrivastava, M., Andreae, M. O., Artaxo, P., Barbosa, H. M. J., Berg, L. K., Brito, J., Ching, J., Easter, R. C., Fan, J., Fast, J. D.,

Feng, Z., Fuentes, J. D., Glasius, M., Goldstein, A. H., Alves, E. G., Gomes, H., Gu, D., Guenther, A., Jathar, S. H., Kim, S., Liu, Y., Lou, S., Martin, S. T., McNeill, V. F., Medeiros, A., de Sa, S. S., Shilling, J. E., Springston, S. R., Souza, R. A. F., Thornton, J. A., Isaacman-VanWertz, G., Yee, L. D., Ynoue, R., Zaveri, R. A., Zelenyuk, A., and Zhao, C.: Urban pollution greatly enhances formation of natural aerosols over the Amazon rainforest, Nat. Commun., 10, 1046, https://doi.org/10.1038/s41467-019-08909-4, 2019.

Song, M., Zhang, C., Wu, H., Mu, Y., Ma, Z., Zhang, Y., Liu, J., and Li, X.: The influence of OH concentration on SOA formation from isoprene photooxidation, Sci. Total Environ., 650, 951–957, https://doi.org/10.1016/j.scitotenv.2018.09.084, 2019.

Surratt, J. D., Lewandowski, M., Offenberg, J. H., Jaoui, M., Kleindienst, T. E., Edney, E. O., and Seinfeld, J. H.: Effect of acidity on secondary organic aerosol formation from isoprene, Environ. Sci. Technol., 41, 5363–5369, https://doi.org/10.1021/es0704176, 2007.

Surratt, J. D., Chan, A. W. H., Eddingsaas, N. C., Chan, M., Loza, C. L., Kwan, A. J., Hersey, S. P., Flagan, R. C., Wennberg, P. O., and Seinfeld, J. H.: Reactive intermediates revealed in secondary organic aerosol formation from isoprene, P. Natl. Acad. Sci. USA, 107, 6640–6645, https://doi.org/10.1073/pnas.0911114107, 2010.

Wang, D. S. and Ruiz, L. H.: Secondary organic aerosol from chlorine-initiated oxidation of isoprene, Atmos. Chem. Phys., 17, 13491–13508, https://doi.org/10.5194/acp-17-13491-2017, 2017.

Wang, J., Ye, J., Zhang, Q., Zhao, J., Wu, Y., Li, J., Liu, D., Li, W., Zhang, Y., Wu, C., Xie, C., Qin, Y., Lei, Y., Huang, X., Guo, J., Liu, P., Fu, P., Li, Y., Lee, H. C., Choi, H., Zhang, J., Liao, H., Chen, M., Sun, Y., Ge, X., Martin, S. T., and Jacob, D. J.: Aqueous production of secondary organic aerosol from fossil-fuel emissions in winter Beijing haze, P. Natl. Acad. Sci. USA, 118, e2022179118, https://doi.org/10.1073/pnas.2022179118, 2021a.

Wang, J., Ye, J., Zhang, Q., Zhao, J., Wu, Y., Li, J., Liu, D., Li, W., Zhang, Y., Wu, C., Xie, C., Qin, Y., Lei, Y., Huang, X., Guo, J., Liu, P., Fu, P., Li, Y., Lee, H. C., Choi, H., Zhang, J., Liao, H., Chen, M., Sun, Y., Ge, X., Martin, S. T., and Jacob, D. J.: Aqueous production of secondary organic aerosol from fossil-fuel emissions in winter Beijing haze, P. Natl. Acad. Sci. USA, 118, e2022179118, https://doi.org/10.1073/pnas.2022179118, 2021b.

Wang, S., Du, L., Tsona, N. T., Jiang, X., You, B., Xu, L., Yang, Z., and Wang, W.: Effect of NO_x and SO_2 on the photooxidation of methylglyoxal: Implications in secondary aerosol formation, J. Environ. Sci. China, 92, 151–162, https://doi.org/10.1016/j.jes.2020.02.011, 2020.

Wang, X., Jacob, D. J., Downs, W., Zhai, S., Zhu, L., Shah, V., Holmes, C. D., Sherwen, T., Alexander, B., Evans, M. J., Eastham, S. D., Neuman, J. A., Veres, P. R., Koenig, T. K., Volkamer, R., Huey, L. G., Bannan, T. J., Percival, C. J., Lee, B. H., and Thornton, J. A.: Global tropospheric halogen (Cl, Br, I) chemistry and its impact on oxidants, Atmos. Chem. Phys., 21, 13973–13996, https://doi.org/10.5194/acp-21-13973-2021, 2021c.

Wen, L., Chen, T., Zheng, P., Wu, L., Wang, X., Mellouki, A., Xue, L., and Wang, W.: Nitrous acid in marine boundary layer over eastern Bohai Sea, China: Characteristics, sources, and implications, Sci. Total Environ., 670, 282–291, https://doi.org/10.1016/j.scitotenv.2019.03.225, 2019.

Wu, X., Xu, L. L., Hong, Y. W., Chen, J. F., Qiu, Y. Q., Hu, B. Y., Hong, Z. Y., Zhang, Y. R., Liu, T. T., Chen, Y. T., Bian, Y. H., Zhao, G. Q., Chen, J. S., and Li, M. R.: The air pollution governed by subtropical high in a coastal city in Southeast China: Formation processes and influencing mechanisms, Sci. Total Environ., 692, 1135–1145, https://doi.org/10.1016/j.scitotenv.2019.07.341, 2019.

Wu, X., Li, M., Chen, J., Wang, H., Xu, L., Hong, Y., Zhao, G., Hu, B., Zhang, Y., Dan, Y., and Yu, S.: The characteristics of air pollution induced by the quasi-stationary front: Formation processes and influencing factors, Sci. Total Environ., 707, 136194, https://doi.org/10.1016/j.scitotenv.2019.136194, 2020.

Xiao, Y., Wu, Z., Guo, S., He, L., Huang, X., and Hu, M.: Formation mechanism of secondary organic aerosol in aerosol liquid water: A review, Chinese Sci. Bull., 65, 3118–3133, 2020.

Xu, L., Guo, H. Y., Boyd, C. M., Klein, M., Bougiatioti, A., Cerully, K. M., Hite, J. R., Isaacman-VanWertz, G., Kreisberg, N. M., Knote, C., Olson, K., Koss, A., Goldstein, A. H., Hering, S. V., de Gouw, J., Baumann, K., Lee, S. H., Nenes, A., Weber, R. J., and Ng, N. L.: Effects of anthropogenic emissions on aerosol formation from isoprene and monoterpenes in the southeastern United States, P. Natl. Acad. Sci. USA, 112, 37–42, https://doi.org/10.1073/pnas.1417609112, 2015.

Xu, L., Du, L., Tsona, N. T., and Ge, M. F.: Anthropogenic Effects on Biogenic Secondary Organic Aerosol Formation, Adv. Atmos. Sci., 38, 1053–1084, https://doi.org/10.1007/s00376-020-0284-3, 2021.

Yang, W., Cao, J., Wu, Y., Kong, F., and Li, L.: Review on plant terpenoid emissions worldwide and in China, Sci. Total Environ., 787, 147454, https://doi.org/10.1016/j.scitotenv.2021.147454, 2021.

Zhang, J., An, J., Qu, Y., Liu, X., and Chen, Y.: Impacts of potential HONO sources on the concentrations of oxidants and secondary organic aerosols in the Beijing-Tianjin-Hebei region of China, Sci. Total Environ., 647, 836–852, https://doi.org/10.1016/j.scitotenv.2018.08.030, 2019.

Zhang, P., Chen, T., Liu, J., Liu, C., Ma, J., Ma, Q., Chu, B., and He, H.: Impacts of SO_2, Relative Humidity, and Seed Acidity on Secondary Organic Aerosol Formation in the Ozonolysis of Butyl Vinyl Ether, Environ. Sci. Technol., 53, 8845–8853, https://doi.org/10.1021/acs.est.9b02702, 2019.

Zhang, Y., Chen, Y., Lei, Z., Olson, N. E., Riva, M., Koss, A. R., Zhang, Z., Gold, A., Jayne, J. T., Worsnop, D. R., Onasch, T. B., Kroll, J. H., Turpin, B. J., Ault, A. P., and Surratt, J. D.: Joint Impacts of Acidity and Viscosity on the Formation of Secondary Organic Aerosol from Isoprene Epoxydiols (IEPDX) in Phase Separated Particles, Acs Earth Space Chem., 3, 2646–2658, https://doi.org/10.1021/acsearthspacechem.9b00209, 2019.

Zhang, Y.-Q., Chen, D.-H., Ding, X., Li, J., Zhang, T., Wang, J.-Q., Cheng, Q., Jiang, H., Song, W., Ou, Y.-B., Ye, P.-L., Zhang, G., and Wang, X.-M.: Impact of anthropogenic emissions on biogenic secondary organic aerosol: observation in the Pearl River Delta, southern China, Atmos. Chem. Phys., 19, 14403–14415, https://doi.org/10.5194/acp-19-14403-2019, 2019.

Zhao, D., Schmitt, S. H., Wang, M., Acir, I.-H., Tillmann, R., Tan, Z., Novelli, A., Fuchs, H., Pullinen, I., Wegener, R., Rohrer, F., Wildt, J., Kiendler-Scharr, A., Wahner, A., and Mentel, T. F.: Effects of NO_x and SO_2 on the secondary organic aerosol formation from photooxidation of α-pinene and limonene, At-

mos. Chem. Phys., 18, 1611–1628, https://doi.org/10.5194/acp-18-1611-2018, 2018.

Zheng, G., Su, H., Wang, S., Andreae, M. O., Pöschl, U., and Cheng, Y.: Multiphase buffer theory explains contrasts in atmospheric aerosol acidity, Science, 369, 1374, https://doi.org/10.1126/science.aba3719, 2020.

Zhou, M., Zheng, G., Wang, H., Qiao, L., Zhu, S., Huang, D., An, J., Lou, S., Tao, S., Wang, Q., Yan, R., Ma, Y., Chen, C., Cheng, Y., Su, H., and Huang, C.: Long-term trends and drivers of aerosol pH in eastern China, Atmos. Chem. Phys. Discuss. [preprint], https://doi.org/10.5194/acp-2021-455, in review, 2021.

Zhu, J., Penner, J. E., Yu, F., Sillman, S., Andreae, M. O., and Coe, H.: Decrease in radiative forcing by organic aerosol nucleation, climate, and land use change, Nat. Commun., 10, 423, https://doi.org/10.1038/s41467-019-08407-7, 2019.